AIChE

Ablative Heat Transfer in a Shrinking Packed-Bed of ZnO Undergoing Solar Thermal Dissociation

L. O. Schunk
Solar Technology Laboratory, Paul Scherrer Institute, Villigen PSI 5232, Switzerland

W. Lipiński
Dept. of Mechanical Engineering, University of Minnesota, Minneapolis, MN 55455

A. Steinfeld
Dept. of Mechanical and Process Engineering, ETH Zurich, Zurich 8092, Switzerland

DOI 10.1002/aic.11782
Published online June 3, 2009 in Wiley InterScience (www.interscience.wiley.com).

A transient heat transfer model is formulated for a shrinking packed-bed of reacting ZnO particles exposed to concentrated solar irradiation. The model combines conduction, convection, and radiation heat transfer with simultaneous sintering and reaction kinetics. Validation is accomplished in terms of temperatures and dissociation rates experimentally measured using a solar-driven thermogravimeter with ZnO packed-bed samples subjected to solar flux concentration ratios in the range 1225–2133 suns and surface temperatures in the range 1834–2109 K. Operating conditions are typical of an ablation regime controlled by the rate of radiative heat transfer to the first layers of ZnO undergoing endothermic dissociation. © 2009 American Institute of Chemical Engineers *AIChE J,* 55: 1659–1666, 2009
Keywords: zinc oxide, dissociation, packed-bed, shrinking, ablation, sintering, radiation, conduction, convection, heat transfer, concentrated, solar energy

Introduction

Solar thermochemical processes for hydrogen production make use of concentrated solar radiation as the energy source of high-temperature process heat.[1] Several 2-step H_2O-splitting thermochemical cycles based on metal oxide redox reactions are being considered.[2–5] Of special interest is the one based on the ZnO/Zn redox reactions, comprising of a 1st step solar endothermic dissociation of ZnO(s), followed by a 2nd step nonsolar exothermic hydrolysis of Zn, and represented by:

$$\text{1st step (solar ZnO-dissociation):}\quad ZnO \rightarrow Zn + 0.5O_2, \quad (1)$$

$$\text{2nd step (nonsolar Zn-hydrolysis):}\quad Zn + H_2O \rightarrow ZnO + H_2. \quad (2)$$

This cycle has been identified as a promising path for solar hydrogen production from water because of its potential of reaching high energy conversion efficiencies and, consequently, economic competitiveness.[6,7] Recently, a 10 kW solar chemical reactor prototype was experimentally demonstrated in a solar furnace.[8] This reactor features a rotating cavity-receiver lined by a packed-bed of ZnO particles that are directly exposed to concentrated solar radiation and serve simultaneously the functions of radiant absorbers, thermal

Correspondence concerning this article should be addressed to A. Steinfeld at aldo.steinfeld@eth.ch

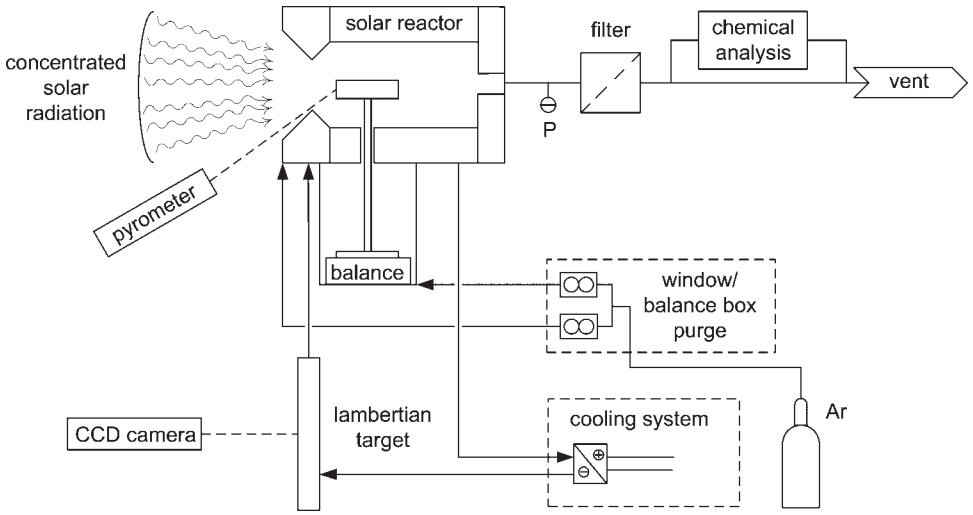

Figure 1. Solar-driven thermogravimeter and experimental set-up at PSI's solar furnace.

insulators, and chemical reactants. As for the 2nd step of the cycle, it has been experimentally demonstrated using an aerosol-flow reactor for in-situ formation and hydrolysis of Zn nanoparticles.[9]

The fundamental understanding of the heat and mass transfer phenomena occurring within a packed-bed of reacting ZnO particles subjected to extreme solar reactor conditions (temperatures > 2000 K and heating rates > 100 K s^{-1}) required the development of a novel solar-driven thermogravimeter that approaches the heat and mass transfer characteristics existing in the solar reactor and further enables on-line monitoring of the weight loss of ZnO as a function of time, temperature, and solar radiative flux. In the previous article (Schunk and Steinfeld, 2009[10]), we described the design and experimentation of such a unique device for the accurate determination of the reaction kinetics. This paper extends the previous kinetic analysis to an energy/mass transport model of a packed-bed reactor that couples the rates of radiation, conduction, and convection heat transfer with the rate of the reaction. The experimental data obtained with the solar-driven thermogravimeter is used for the determination of the thermal transport properties of the ZnO packed-bed and for validating the packed-bed reactor model.

Experimental set-up

The solar-driven thermogravimetry (solar TG) and the experimental set-up are shown schematically in Figure 1. The solar TG's design and fabrication has been previously described in detail (Schunk and Steinfeld,[10]), the most important features are summarized here. The main component is a 152 mm-i.d. 150 mm-length cavity-receiver, lined with CaO-stabilized ZrO_2 bricks over porous Al_2O_3 insulation, and containing a 60 mm-diameter circular opening-the aperture-to let in concentrated solar energy through a transparent 3-mm-thick quartz window. Inside the cavity, ZnO samples are mounted on an Al_2O_3 rod that is suspended on a balance. With this arrangement, the ZnO sample is directly exposed to concentrated solar radiation while its weight loss is continuously monitored during decomposition. An Ar flow, injected tangentially and radially at the aperture plane, creates an aerodynamic curtain that protects the window from condensable products and carries the gaseous products, Zn(g) and O_2, to the outlet port at the rear of the cavity. The Zn(g) is condensed and filtered downstream, and the off-gas composition is then analyzed. Recombination of the gaseous products was avoided and Zn yields exceeding 90% were obtained by incorporating a quenching unit at the solar TG's outlet port.[11]

Experimentation was carried out at PSI's solar furnace[12]: a sun-tracking flat heliostat on-axis with a stationary primary parabolic concentrator. Solar flux intensities, regulated with a Venetian-type shutter located between the heliostat and the solar concentrator, were measured optically with a calibrated CCD camera on a water-cooled Al_2O_3-plasma coated Lambertian target. The CCD camera also allowed for sample visualization during experimental runs. Samples can be exposed to peak solar flux concentration ratios exceeding 5000 suns* and can reach temperatures above 2500 K at heating rates of 1000 K s^{-1}. Sample's surface temperatures were measured with a solar blind pyrometer (measurement range 773–2773 K) that is not affected by the reflected solar irradiation because measurements are taken in a narrow wavelength interval around 1.39 μm where solar irradiation is mostly absorbed by the atmosphere.[13]

Two types of samples were examined; they are shown schematically in Figure 2. Both were introduced in a 20-mm-i.d. and 40-mm-length Al_2O_3 tube. Sample 1 (Figure 2a) consisted of a 3.7-mm-thick sintered ZnO tile followed by a 36.3-mm-thick 80%Al_2O_3–20%SiO_2 porous insulation. Sample 2 (Figure 2b) consisted of a 12-mm-thick packed-bed of ZnO powder, followed by a 3.7-mm-thick sintered ZnO tile and 24.3-mm-thick 80%Al_2O_3–20%SiO_2 porous insulation. Sample 1 was used to determine the thermal transport properties. Sample 2 represented exactly the configuration encountered in the 10 kW solar reactor[8] and was used to

*Solar concentration ratio is defined as the mean solar radiative flux over the aperture normalized to 1 kW m^{-2}, and is usually given in units of "suns".

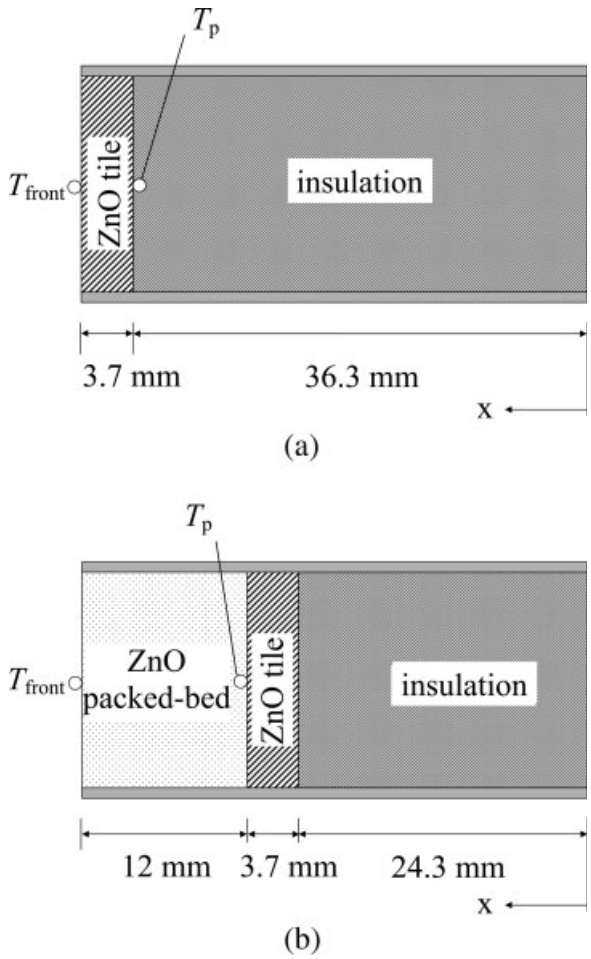

Figure 2. ZnO samples investigated: (a) sample 1, (b) sample 2.

Indicated are temperature measurement locations T_p (type-B thermocouple) and T_{front} (solar-blind pyrometry).

validate the heat transfer model. The total mass and mean initial porosity of the ZnO packed-bed were 6.2 g and 70%, respectively. Particle size distribution was measured by laser scattering (HORIBA LA-950 analyzer). BET specific surface area (SSA) was measured by N_2 adsorption at 77 K (Micromeritics 3000). SEM pictures of the ZnO powder (Alpha Aesar 11558, mean particle size = 0.96 μm, SSA = 6.23 m^2 g^{-1}) and the ZnO tile (ALPHA Ceramics, purity 99.8 wt %, bulk density 5550 kg m^{-3}) are shown in Figures 3a, b, respectively. The grain size of the sintered ZnO is in the range of 2–8 μm. Grain boundaries are visible as well as an example of an embedded pore in the upper right of Figure 3b.

Heat transfer model

Mass conservation—The unsteady mass conservation equation is given by:

$$\frac{d\, n_{ZnO}}{dV dt} = r''' \tag{3}$$

where dV is a differential volume of ZnO shrinking with time as the sample undergoes sintering and thermal dissociation. The ZnO dissociation rate is modeled by applying a zero-order Arrhenius-type rate law (Schunk and Steinfeld,[10]),

$$r''' = -ak_0 \exp\left(-\frac{E_a}{RT}\right) \tag{4}$$

where a is the specific surface area. The kinetic parameters $k_0 = 172.13 \times 10^6$ mol m^{-2} s^{-1} and $E_a = 361$ kJ mol^{-1} were determined using the solar TG for ZnO samples directly irradiated in a solar furnace (Schunk and Steinfeld,[10]).

Energy conservation—The unsteady 1D energy conservation equation is given by:

$$\rho c_p \frac{\partial T}{\partial t} = \nabla(k_{eff}\nabla T) + q'''_{radiative} - \Psi(t)\varepsilon_{lateral}\sigma(T^4 - T^4_{cavity}) + q'''_{chemistry} \tag{5}$$

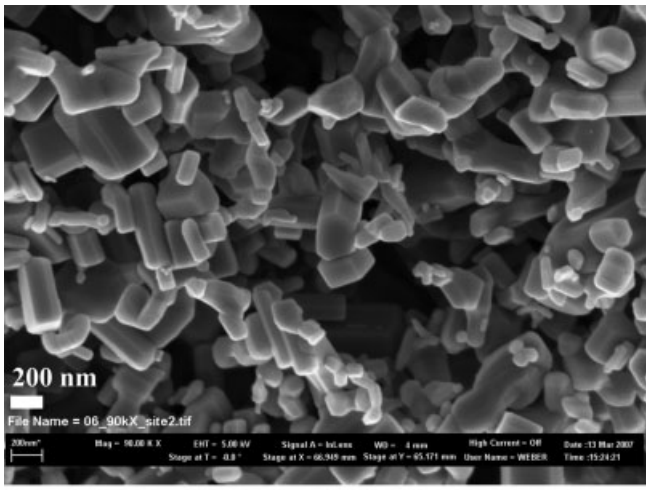

(a)

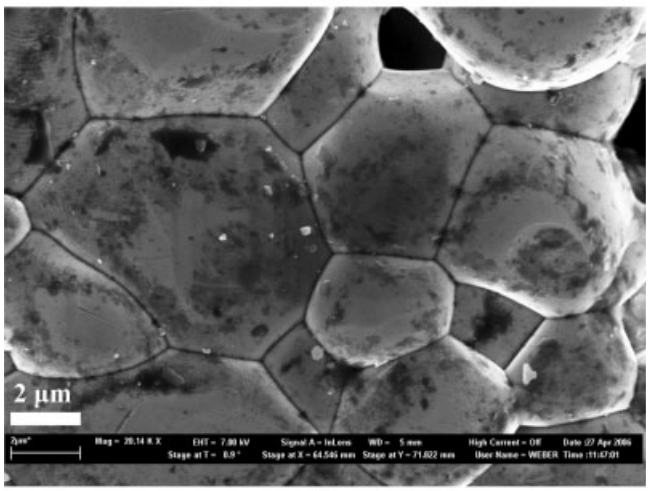

(b)

Figure 3. SEM of (a) ZnO powder (Alpha Aesar 11558, mean particle size = 0.96 μm, SSA = 6.23 m^2 g^{-1}), and (b) ZnO tile (ALPHA Ceramics, purity 99.8 wt %, bulk density 5550 kg m^{-3}).

$\Psi(t)$ is the lateral surface area to volume ratio of the cylindrical sample. $q'''_{\text{radiative}}$ denotes the net radiative heat per unit volume that is absorbed at the surfaces of the inner volumes directly exposed to external radiation (solar + surroundings),

$$q'''_{\text{radiative}} = \frac{A}{V}[\alpha_s q''_{\text{solar}} - \sigma\varepsilon(T^4 - T^4_{\text{cavity}})] \tag{6}$$

where q''_{solar} is the incident solar flux and A represents the irradiated surface area between incremental volumes of different diameter. $q'''_{\text{chemistry}}$ is the volumetric heat sink rate due to the endothermic ZnO dissociation given by the product of the reaction rate and the enthalpy change (in J mol^{-1}),[14]

$$\begin{aligned} q'''_{\text{chemistry}} &= r'''\Delta H_r(T) \\ &= r'''(4.851 \times 10^5 - 13.13\,T - 2.164 \times 10^{-3}\,T^2) \end{aligned} \tag{7}$$

The boundary conditions are:
at the directly irradiated surface, $x = L(t)$,

$$k_{\text{eff}}\frac{\partial T}{\partial x} = h_{\text{front}}(T_{\text{gas}} - T) + \varepsilon\sigma(T^4_{\text{cavity}} - T^4) + \alpha_{\text{solar}} q''_{\text{solar}} \tag{8}$$

at the back surface, $x = 0$,

$$k_{\text{eff}}\frac{\partial T}{\partial x} = \varepsilon\sigma(T^4 - T^4_{\text{cavity}}) \tag{9}$$

The initial condition is:

$$T(x, t = 0) = T_0 \tag{10}$$

The effective thermal conductivity is given by the sum of the conductive and radiative contributions, $k_{\text{eff}} = k_{\text{conductive}} + k_{\text{radiative}}$. For the optically-thick packed-bed, the Rosseland diffusion approximation is applied,[15]

$$k_{\text{radiative}} = \frac{16n^2}{3\beta}\sigma T^3 \tag{11}$$

$k_{\text{conductive}}$ decreases from 27 to 6 W m^{-1} K^{-1} in the interval 295–973 K for hot-pressed ZnO powder,[16] and from 37 to 4 W m^{-1} K^{-1} in the interval 295–1273 K for fully sintered ZnO.[17] The latter results are used in this study with exponential fit, $k_{\text{conductive}}(T) = 59.145 \cdot e^{-2\times10^{-3}T}$ W m^{-1} K^{-1}. The thermal conductivity of the porous packed-bed of ZnO particles, is given by[17]

$$\begin{aligned} k_{\text{conductive,porous}} = k_{\text{gas}}\Bigg[1 - \sqrt{1-p} + \sqrt{1-p}\,\frac{2}{1-\varphi B} \\ \times\left(\frac{(1-\varphi)B}{(1-\varphi B)^2}\ln\frac{1}{\varphi B} - \frac{B+1}{2} - \frac{B-1}{1-\varphi B}\right)\Bigg] \end{aligned} \tag{12}$$

where $\varphi = k_{\text{gas}}/k_{\text{conductive}}$, the porosity p of the batch is calculated in the following section, and the deformation factor for spherical particles is $B = 1.25(1 - p/p)^{\frac{10}{9}}$.[18] The spectral emissivity of ZnO is assumed constant over the entire spectral and temperature ranges considered in the present study, and equal to 0.69 as measured at 1.39 μm and 2000 K.[19] The absorptivity on the other hand is assumed to increase with temperature (see Results). The convective heat transfer coefficient h_{front} is obtained by employing the Nu correlation for a circular disc exposed to a perpendicular fluid flow,[20]

$$Nu = \frac{8}{\sqrt{2\pi}}\left(\frac{2d_{\text{aperture}}}{d_{\text{cylinder}}}\right)^{1/2}\left(\frac{d_{\text{aperture}}RePr}{4L_{\text{front-aperture}}} - \frac{2d_{\text{cylinder}}}{d_{\text{aperture}}}\right)^{1/2} \tag{13}$$

The characteristic lengths for Nu and Re are based on the cylinder diameter d_{cylinder}, aperture diameter d_{aperture}, and the distance between the cylinder front surface and aperture $L_{\text{front-aperture}}$. Convective heat transfer at the lateral and back surfaces is assumed negligible as compared to radiative heat transfer between these surfaces and the cavity walls, and hence omitted from consideration. The variation of heat capacities and thermal conductivities of the insulation materials were incorporated as a function of temperature.[21,22] The finite volume method and the explicit Euler time integration scheme are applied for solving Eqs. 3 and 5, which are integrated over shrinking circular disc elements ΔV and over a finite time step Δt. The rates of shrinking in the radial and axial directions are determined independently for each finite volume based on the rates of sintering and ZnO-dissociation, as elaborated in the next section.

Sintering is assumed to be isotropic and following three idealized, sequential stages.[23,24] Transitions from the initial to the intermediate and final stages occur at relative densities $\rho/\rho_p = 0.65$ and 0.95, respectively.[25] In each stage, lattice diffusion from the grain boundary is assumed to be the controlling mechanism with suppressed grain growth, as observed experimentally for microwave-sintered ZnO samples subjected to heating rates comparable to those in this study.[26] Grains are assumed to have tetrakaidecahedronal shape. In the initial stage, the density and the relative linear shrinkage $Y = (L - L_0)/L_0$ (where L is either x or d) are obtained from[25]:

$$\rho = \rho_0(1+Y)^{-3}, \quad Y = \left(\frac{80\pi D\gamma_{sv}\Omega}{2^b(G/2)^a k_B T}t\right)^{2/b}, \tag{14}$$

where $G = 14$ μm is the grain size, $\gamma_{sv} = 1$ J m^{-2} is the specific surface energy of ZnO,[27] k_B is the Boltzmann constant, and $\Omega = 2.4 \times 10^{-29}$ m^3 is the vacancy volume of ZnO.[26] D is the diffusion coefficient, obtained by fitting to a lattice diffusion model,[28] $D = 1.72 \cdot e^{-\frac{(276\pm13)\text{kJ mol}^{-1}}{RT}}\text{m}^2\text{s}^{-1}$. In the intermediate and final stages, the density variation due to sintering is obtained from[25]:

$$\frac{1}{\rho}\frac{d\rho}{dt} = \frac{40}{3}\left(\frac{D\Omega}{G^a k_B T}\right)\left(\frac{b\gamma_{sv}}{r_p}\right) \tag{15}$$

Coefficients a and b of Eqs. 14 and 15 are listed in Table 1. r_p is the mean pore size approximated by $r_p \approx 0.1967\sqrt{p}G$.[25] The linear shrinkage in the intermediate

Table 1. Coefficients a and b in Eqs. 14 and 15 for Initial, Intermediate, and Final Stages of the Sintering Model[26]

	Initial Stage	Intermediate Stage	Final Stage
a	3	2	2
b	5	1	2

and final stages is due to the combined sintering and mass change due to the chemical reaction. Thus,

$$\frac{dx}{dt} = \frac{x}{d}\frac{dd}{dt} = \frac{4\Delta V\left(\frac{d\rho}{dt} - r'''M\right)}{3\rho\pi d^2} \tag{16}$$

where ΔV is the size of a finite volume.

Results

Radiative properties

A selected solar experimental run is performed with sample 1 to determine the extinction coefficient β and the surface absorptance α_{solar} for dense ZnO by fitting the numerically calculated temperatures to those experimentally measured. In this specific run, dissociation is neglected because temperatures were kept below 1810 K and the final measured reaction extent was only 0.65%. β is assumed to be constant. α_{solar}, is assumed to be proportional to the values of the mean gray scale intensity I of the irradiated surface, measured online with the CCD camera,

$$\alpha_{solar} = \alpha_{solar,min} + (I_{max} - I(t))\frac{\alpha_{solar,max} - \alpha_{solar,min}}{I_{max} - I_{min}}. \tag{17}$$

The sample is exposed to a step-wise increasing solar flux q''_{solar} ranging from 0.16 to 0.90 MW m^{-2}, as shown in Figure 4. The measured and computed temperatures T_{front} and T_p are also shown in Figure 4. Best fit was obtained for $\beta = 1900$ m^{-1}, $\alpha_{solar,min} = 0.15$, and $\alpha_{solar,max} = 0.95$. The values of $\alpha_{solar,min}$ at 295 K and $\alpha_{solar,max}$ at 2000 K are consistent with previous reports.[29,30] The value of β is lower than that for a mixture of ZnO and C at room temperature,[31] most likely due the different composition and temperatures, along with the uncertainty of $k_{conductive}$. The extinction coefficient of the porous packed-bed is computed as $\beta_{porous} = (1 - p)\beta$.[32] For $p = 0$ and $T \geq 1200$ K,

$$k_{eff}(T) = 59.145e^{-2\times10^{-3}\,T} + 3.02 \times 10^{-10}\,T^3 \tag{18}$$

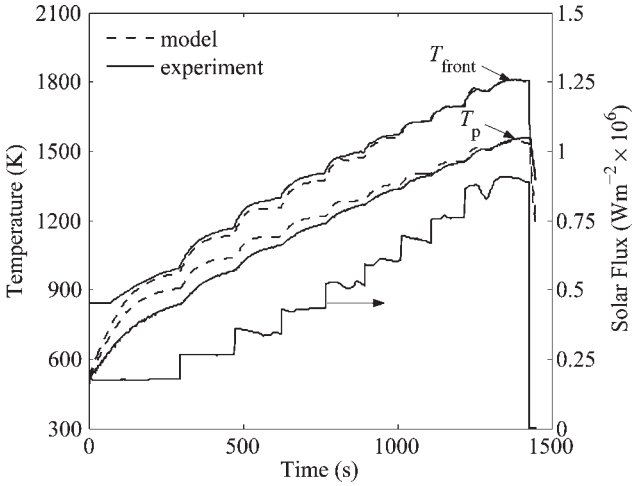

Figure 4. Experimentally measured incident solar flux, experimentally measured and numerically calculated temperatures on the irradiated front surface T_{front}, and behind the ZnO tile T_p, as a function of time for sample 1.

Table 2. Irradiated Surface Temperature T_{front}, Peak Solar Flux Concentration Ratio C, Maximum Mean Solar Flux $q''_{solar,max}$, and Mean Mass Loss Rate dm/dt for the Solar Experimental Runs with Sample 2 at PSI's Solar Furnace

Run	T_{front} (K)	C_{max} (suns)	$q''_{solar,max}$ (kW m^{-2})	dm/dt (mg s^{-1})
1	2109.1	2133	1662	2.71
2	1977.8	1574	1222	0.52
3	1889.8	1517	1177	0.32
4	1902.1	1411	1095	0.28
5	1833.6	1225	949	0.09
6	2038.6	1837	1429	1.09
7	1945.6	1493	1157	0.38

Temperatures and chemical conversion

Seven solar experimental runs with sample 2 were carried out; their operational conditions are listed in Table 2. The specific surface area $a = 840$ m^{-1} of the rate law, Eq. 4, was iteratively found by fitting experimentally measured and numerically calculated dissociation rates for all 7 runs, as shown in the Arrhenius-type plot of Figure 5. Measured and calculated temperatures and weight loss for runs No. 2 and 3 are shown as a function of time in Figure 6 a and b, respectively. The sample was subjected to a stepwise increasing solar flux with $q''_{solar,max} = 1.22$ MW m^{-2}, whereas $q''_{solar,max} = 1.17$ MW m^{-2} was applied during run No. 3 at $t = 0$ s. The

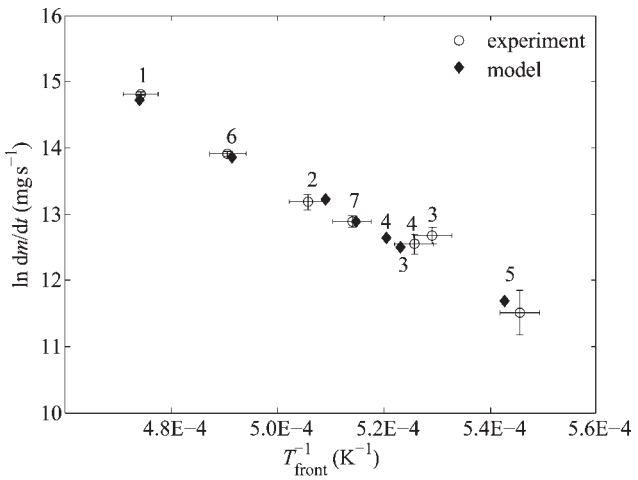

Figure 5. Arrhenius plot for the experimentally measured and numerically calculated reaction rates.

The solar run numbers are indicated by labels adjacent to the data points.

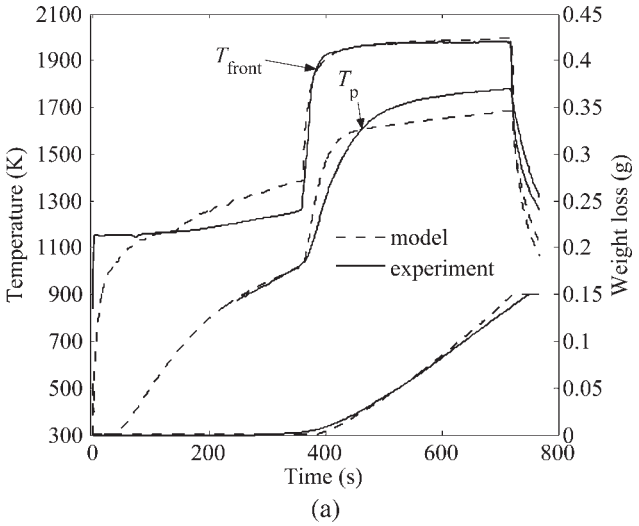

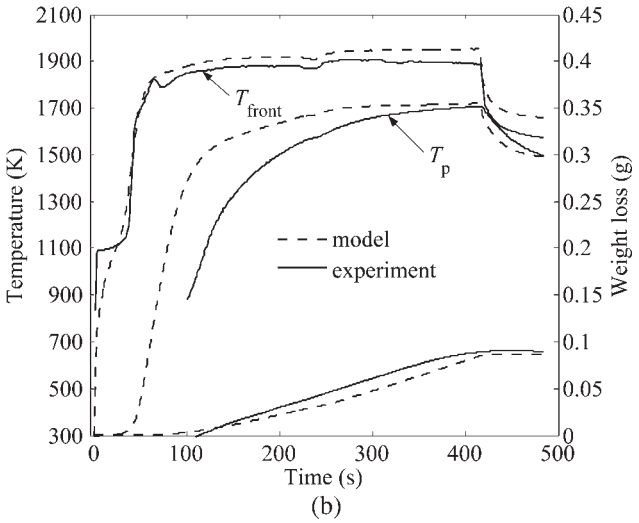

Figure 6. Experimentally measured and numerically calculated temperatures on the irradiated front surface T_{front}, and behind the ZnO tile T_p, and weight loss as a function of time for runs (a) No. 2 and (b) No. 3.

agreement for T_{front} is reasonable well for both runs. The sudden increase for run No. 2 at $t = 362$ s is due to an increase in q''_{solar} from 0.64 to 1.21 MW m^{-2}, while the sudden decrease for run No. 3 at $t = 416$ s is due to the termination of the run and interruption of q''_{solar}. Discrepancy between measured and calculated T_p is observed during the initial stages, attributed to an overestimation of the sintering rate, which in turn resulted in an overestimation of k_{eff} and, consequently, faster heating of the packed-bed of ZnO particles. On the other hand, the model is able to predict with good accuracy the weight loss, occurring at $T_{front} > 1000$ K.

The temperature profiles across the packed are shown in Figure 7 for run No. 3. The parameter is the reaction time, $t = 10$–400 s. Shrinking due to sintering and dissociation is clearly observed. The front surface retraces from its axial position $x = 0.04$ m to 0.037 m in the first 100 s due mainly to shrinkage, and afterwards due mainly to dissociation as

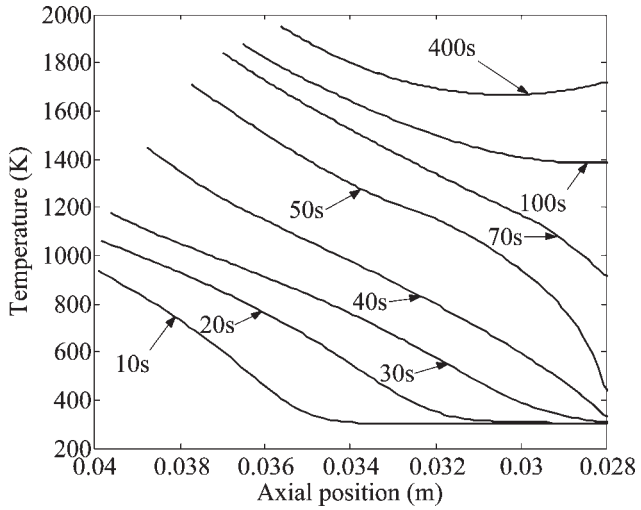

Figure 7. Modeled temperature profiles across the ZnO packed-bed of ZnO powder at times t = 10, 20, 30, 40, 50, 70, 100, and 400 s for run No. 3.

T_{front} exceeds 1878 K. The advance of sintering is also manifested by the change of k_{eff} and the temperature gradients across the packed-bed. Evidently, as sintering progresses and the bed shrinks, p decreases and k_{eff} increases, resulting in low ΔT across the bed.

The local dissociation rates across the packed-bed for run No. 3 are shown in Figure 8, along with the cumulative dissociation, defined as:

$$X(x,t) = \frac{\int_x^L d^2 r''' dx}{\int_0^L d^2 r''' dx}. \tag{19}$$

The parameter is the reaction time, $t = 100$, 200, 300, and 400 s. As expected, the maximum dissociation rate r'''_{max} is

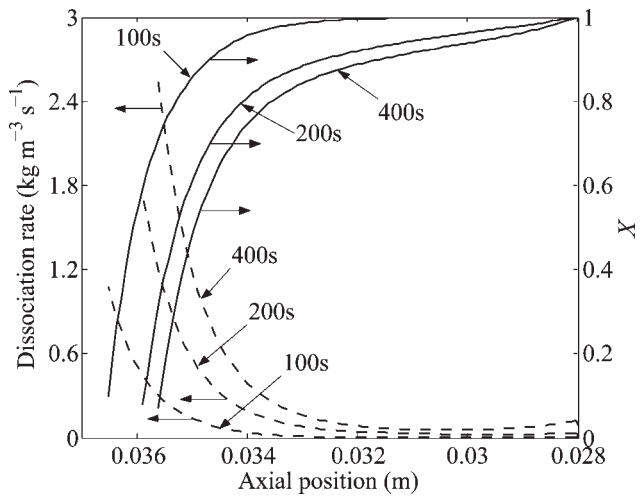

Figure 8. Modeled dissociation rate and cumulative dissociation across the ZnO packed-bed at t = 100, 200, and 400 s for run No. 3.

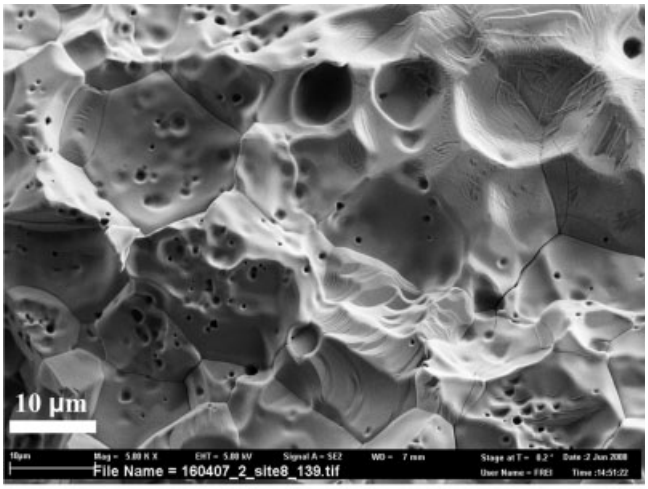

(a)

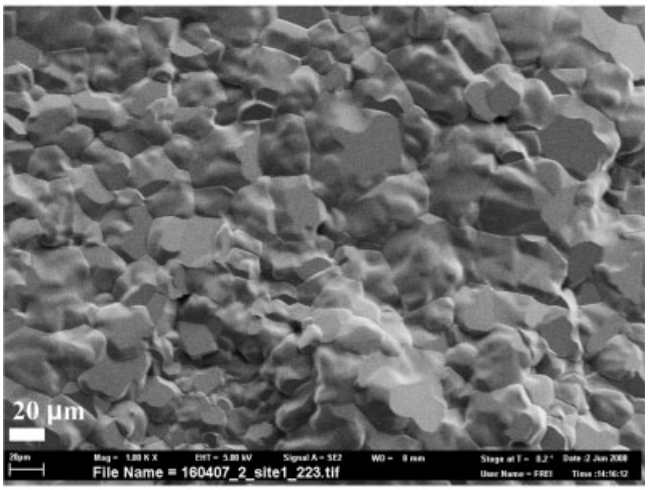

(b)

Figure 9. SEM of the product sample after the solar run No. 3 for: (a) a layer near the irradiated surface, and (b) layer in the vicinity of the ZnO tile at $x = 0.029$ m.

found at the front layer exposed to direct solar irradiation, where temperature is highest. However, it decreases rapidly towards the inner layers as a result of the Arrhenius dependency. r'''_{max} increases from 1.08 kg m^{-3} s^{-1} at $t = 100$ to 2.55 kg m^{-3} s^{-1} at $t = 400$ s as the temperature of the entire packed-bed increases. Interestingly, X rapidly drops in the first few millimeters since most of the dissociation reaction occurs there. For example, at $t = 100$ s, 92% of the reaction occurs within an active layer of 2 mm thickness The active layer thickness increases with time and temperature: at $t = 400$ s, 90% of the reaction occurs within the first 4 mm of the sample. Thus, the packed-bed is subjected to an ablation regime controlled by the rate of heat transfer by radiation to the endothermic reaction. The active layer corresponds approximately to the thickness of the ablated surface region of the sample, which contains small cracks, needles, and ridges. SEM images of the product sample after the solar run No. 3 are shown in Figure 9 for: a) a layer near the irradiated surface, and b) a layer in the vicinity of the ZnO tile at $x = 0.029$ m. The irradiated surface exhibits pores and cracks, suggesting that product gases Zn(g) and O_2 can escape through these cracks and ridges, bypassing the limitation imposed by diffusion through small pores at the dense regions of the bed. The deeper layer is fully sintered and is characterized by grain sizes in the range 5–30 μm.

Conclusions

A 1D transient numerical model has been developed for simulating an irradiated packed-bed of ZnO particles undergoing sintering and thermal dissociation. The governing mass and energy conservation equations that couple the radiative, conductive, and convective heat transfer to the kinetic rate of the dissociation reaction were formulated and solved numerically by the finite volume method using the explicit Euler time integration scheme. The thermal transport properties, namely the extinction coefficient, the surface absorptivity, and the effective thermal conductivity were obtained by fitting measured and calculated temperatures for a selected run without reaction. The ZnO dissociation reaction occurred in the topmost layers at the highest temperatures which is typical of an ablation regime, as radiative transfer to the endothermic reaction proceeded at a faster rate than heat conduction across the packed-bed.

Acknowledgements

The authors acknowledge the financial support from the Swiss Federal Office of Energy. They also thank A. Weber and A. Frei for the SEM images, and N. Rotering and K. Cuche for technical support during the experimental campaign at PSI's solar furnace.

Notation

a = specific surface area, m^{-1}
a, b = coefficients in Eqs. 14–15
A = surface area, m^2
B = deformation factor
c_p = specific heat capacity, J mol^{-1} K^{-1}
C = concentration ratio, 1 kW m^{-2}
d = diameter, m
D = diffusion coefficient, m^2 s^{-1}
E_a = activation energy, kJ mol^{-1}
G = grain size, m
h = convective heat transfer coefficient, W m^{-2} K^{-1}
H_r = heat consumption of ZnO dissociation reaction, J mol^{-1}
I = gray scale intensity
k = thermal conductivity, W m^{-1} K^{-1}
k_B = Boltzmann constant, J K^{-1}
k_0 = frequency factor, mol m^{-2} s^{-1}
L = length, m
M = molecular mass, kg mol^{-1}
n = number of moles; index of refraction
Nu = Nusselt number
p = porosity
Pr = Prandtl number
q'' = heat flux, W m^{-2}
q''' = volumetric heat sink/source, W m^{-3}
r = radius, m
r''' = dissociation rate, mol m^3 s^{-1}
R = universal gas constant J mol^{-1} K^{-1}
Re = Reynolds number
t = time, s
T = temperature, K
V = volume, m^3
x = axial position, m

X = cumulative dissociation
Y = linear shrinkage

Greek letters

α = absorptance
β = mean extinction coefficient, m^{-1}
γ_{sv} = specific surface energy, J m^{-2}
ε = emissivity
ρ = density, kg m^{-3}
σ = Stefan-Boltzmann constant, W m^{-2} K^{-4}
Ω = vacancy volume, m^3
Ψ = specific surface area, m^{-1}

Subscripts

eff = effective
p = pore, particle
0 = initial

Literature Cited

1. Steinfeld A. Solar thermochemical production of hydrogen-a review. *Solar Energy*. 2005;78:603–615.
2. Abanades S, Flamant G. Thermochemical hydrogen production from a two-step solar-driven water-splitting cycle based on cerium oxides. *Solar Energy*. 2006;80:1611–1623.
3. Agrafiotis C, Roeb M, Konstandopoulos AG, Nalbandian L, Zaspalis VT, Sattler C, Stobbe P, Steele AM. Solar water splitting for hydrogen production with monolithic reactors. *Solar Energy*. 2005;79: 409–421.
4. Inoue M, Hasegawa N, Uehara R, Gokon N, Kaneko H, Tamaura Y. Solar hydrogen generation with $H_2O/ZnO/MnFe_2O_4$ system. *Solar Energy*. 2004;76:309–315.
5. Kodama T, Nakamuro Y, Mizuno T. A Two-Step Thermochemical water splitting by iron-oxide on stabilized zirconia. *J Solar Energy Eng*. 2006;128:3–7.
6. Haueter P, Moeller S, Palumbo R, Steinfeld A. The production of zinc by thermal dissociation of zinc oxide-solar chemical reactor design. *Solar Energy*. 1999;67:161–167.
7. Perkins C, Weimer AW. Likely near-term solar-thermal water splitting technologies. *Int. J. Hydrogen Energy*. 2004;29:1587–1599.
8. Schunk LO, Haeberling P, Wepf S, Wuillemin D, Meier A, Steinfeld A. A receiver-reactor for the solar thermal dissociation of zinc oxide. *J. Solar Energy Eng*. 2008;130:021009.
9. Ernst FO, Tricoli A, Pratsinis SE, Steinfeld A. co-synthesis of H_2 and ZnO by in-situ Zn aerosol formation and hydrolysis. *AIChE J*. 2006;52:3297–3303.
10. Schunk L, Steinfeld A. Kinetics of the thermal dissociation of ZNO exposed to concentrated solar irradiation using a solar-driven thermogravimeter in the 1800-2100k range. *AICHE J*. 2009;55:1497–1504.
11. Gstoehl D, Brambilla A, Schunk L, Steinfeld A. A quenching apparatus for the gaseous products of the solar thermal dissociation of ZnO. *J Mater Sci*. 2008;43:4729–4736.
12. Haueter P, Seitz T, Steinfeld A. A new high-flux solar furnace for high-temperature thermochemical research. *J Solar Energy Eng*. 1999;121:77–80.
13. Tschudi HR, Morian G. Pyrometric temperature measurements in solar furnaces. *J Solar Energy Eng*. 2001;123:164–170.
14. Roine A. *Outokumpu HCS Chemistry 5.11*. Pori, Finland: Outokumpu Research Oy, 2002.
15. Siegel R, Howell J. *Thermal Radiation Heat Transfer*, 4th ed. New York, London: Taylor & Francis, 2002.
16. Cai KF, Müller E, Drašar C, Mrotzek A. Preparation and thermoelectric properties of Al-doped ZnO ceramics. *Mater Sci Eng B*. 2003;104:45–48.
17. Olorunyolemi T, Birnboim A, Carmel Y, Wilson OC, Lloyd IK. Thermal conductivity of zinc oxide: from green to sintered state. *J Am Ceram Soc*. 2002;85:1249–1253.
18. Zehner P, Schlünder EU. Wärmeleitfähigkeit von Schüttungen bei mäßigen Temperaturen. *Chemie Ingenieur Technik—CIT*. 1970;42: 933–941.
19. Möller S. Entwicklung eines Reaktors zur solarthermischen Herstellung von Zink aus Zinkoxid zur Energiespeicherung mit Hilfe konzentrierter Sonnenstrahlung. PhD Thesis, ETH, Zürich, 2001.
20. Kendoush AA. Theory of convective heat and mass transfer to fluids flowing normal to a plane. *Int Commun Heat Mass Transf*. 1996;23: 249–262.
21. *MPDB*, 5.50. JAHM Software. 1999.
22. Rath Group. Product no.: Kerform KVS 1800/400. Available at: www.rath-group.com.
23. Coble RL. Sintering crystalline solids. I. Intermediate and final state diffusion models. *J Appl Phys*. 1961;32:787–792.
24. Coble RL. Sintering crystalline solids. II. Experimental test of diffusion models in powder compacts. *J Appl Phys*. 1961;32:793–799.
25. Rahaman MN. *Ceramic Processing*. New York: Taylor & Francis Group, 2007.
26. Xu G-f, Lloyd IK, Carmel Y, Olorunyolemi T, Wilson OC. Microwave sintering of ZnO at ultra high heating rates. *J Mater Res*. 2001;16:2850–2858.
27. Gupta TK, Coble RL. Sintering of ZnO. II. Density decrease and pore growth during the final stage of the process. *J Am Ceram Soc*. 1968;51:525–528.
28. Gupta TK, Coble RL. Sintering of ZnO. I. Densification and grain growth. *J Am Ceram Soc*. 1968;51:521–525.
29. Touloukian YS, DeWitt DP, Hernicz RS. *Thermal Radiative Properties*, Vol. 8. New York: IFI/Plenum, 1972.
30. Möller S, Palumbo R. Solar thermal decomposition kinetics of ZnO in the temperature range 1950-2400 K. *Chem Eng Sci*. 2001;56: 4505–4515.
31. Osinga T, Lipinski W, Guillot E, Olalde G, Steinfeld A. Experimental determination of the extinction coefficient for a packed-bed particulate medium. *Exp Heat Transf*. 2006;19:69–79.
32. Dombrovsky LA, Tagne HK, Baillis D, Gremillard L. Near-infrared radiative properties of porous zirconia ceramics. *Infrared Phys Technol*. 2007;51:44–53.

Manuscript received Sept. 3, 2008, and revision received Nov. 1, 2008.